Materials Science and Engineering A368 (2004) 222–230

MATERIALS SCIENCE & ENGINEERING A

www.elsevier.com/locate/msea

Analysis of the impact velocity of powder particles in the cold-gas dynamic-spray process

M. Grujicic [a,*], C.L. Zhao [a], C. Tong [a], W.S. DeRosset [b], D. Helfritch [b]

[a] *Department of Mechanical Engineering, Clemson University, 241 Fluor Daniel Engineering Innovation Building, Clemson, SC 29634, USA*
[b] *Army Research Laboratory—Processing and Properties Branch Aberdeen, Proving Ground, Aberdeen, MD 21005-5069, USA*

Received 16 August 2003; received in revised form 27 October 2003

Abstract

While built on a sound physical foundation, isentropic, one-dimensional models generally used to analyze the dynamics of dilute two-phase (feed-powder particles suspended in a carrier gas) flow during the cold-gas dynamic-spray process, require the use of numerical procedures to obtain solutions for the governing equations. Numerical solutions, unfortunately, do not enable an easy establishment of the relationships between the gas, process and feed-powder parameters on one side and the gas and the particle velocities at the nozzle exit and the particle impact velocity, on the other. Analytical solutions for the governing equations in the limits of small and large relative particle/gas velocities and a multiple non-linear regression analysis are used, in the present work, to develop analytical functions which can be used to compute the gas and the particle exit velocities and the particle impact velocity for a given set of the gas, process, and feed-powder parameters. The results obtained using the analytical functions are found to be in a very good agreement with their numerical and experimental counterparts.

Keywords: Cold-gas; Dynamic-spray; Process design and optimization

1. Introduction

The cold-gas dynamic-spray process, often referred to as simply "cold spray," is a high-rate material deposition process in which fine, solid powder particles (generally 1–50 μm in diameter) are accelerated in a supersonic jet of compressed (carrier) gas to velocities in a range between 500 and 1000 m/s. As the solid particles impact the target surface, they undergo plastic deformation and bond to the surface, rapidly building up a layer of deposited material. Cold spray as a coating technology was initially developed in the mid-1980s at the Institute for Theoretical and Applied Mechanics of the Siberian Division of the Russian Academy of Science in Novosibirsk [1,2]. The Russian scientists successfully deposited a wide range of pure metals, metallic alloys, polymers, and composites onto a variety of substrate materials. In addition, they demonstrated that very high coating deposition rates on the order of 5 m^2/min (∼ 300 ft^2/min) are attainable using the cold-spray process.

A simple schematic of a typical cold-spray device is shown in Fig. 1. Compressed gas of an inlet pressure on the order of 30 bar (500 psi) enters the device and flows through a converging/diverging nozzle to attain a supersonic velocity. The solid powder particles are metered into the gas flow upstream of the converging section of the nozzle and are accelerated by the rapidly expanding gas. To achieve higher gas flow velocities in the nozzle, the compressed gas is often preheated. However, while preheat temperatures as high as 900 K are sometimes used, due to the fact that the contact time of spray particles with the hot gas is quite short and that the gas rapidly cools as it expands in the diverging section of the nozzle, the temperature of the particles remains substantially below the initial gas preheat temperature and, hence, below the melting temperature of the powder material.

The actual mechanism by which the solid particles deform and bond during cold spray is still not well understood. The prevailing theory for cold-spray bonding postulates that, during impact, the solid particles undergo plastic deformation, disrupt thin (oxide) surface films and, in turn, achieve intimate conformal contact with the target surface. The intimate conformal contact combined with high contact pressures

* Corresponding author. Tel.: +1-864-656-5639; fax: +1-864-656-4435.
E-mail address: mica.grujicic@ces.clemson.edu (M. Grujicic).

0921-5093/$ – see front matter © 2003 Elsevier B.V. All rights reserved.
doi:10.1016/j.msea.2003.10.312

Report Documentation Page

Form Approved
OMB No. 0704-0188

1. REPORT DATE	2. REPORT TYPE	3. DATES COVERED
2004		**00-00-2004 to 00-00-2004**

4. TITLE AND SUBTITLE	5a. CONTRACT NUMBER
Analysis of the impact velocity of powder particles in the cold-gas dynamic-spray process	5b. GRANT NUMBER
	5c. PROGRAM ELEMENT NUMBER
6. AUTHOR(S)	5d. PROJECT NUMBER
	5e. TASK NUMBER
	5f. WORK UNIT NUMBER
7. PERFORMING ORGANIZATION NAME(S) AND ADDRESS(ES) **Celmson University,Department of Mechanical Engineering,Clemson,SC,29634**	8. PERFORMING ORGANIZATION REPORT NUMBER
9. SPONSORING/MONITORING AGENCY NAME(S) AND ADDRESS(ES)	10. SPONSOR/MONITOR'S ACRONYM(S)
	11. SPONSOR/MONITOR'S REPORT NUMBER(S)

12. DISTRIBUTION/AVAILABILITY STATEMENT
Approved for public release; distribution unlimited

13. SUPPLEMENTARY NOTES

14. ABSTRACT

While built on a sound physical foundation, isentropic, one-dimensional models generally used to analyze the dynamics of dilute two-phase (feed-powder particles suspended in a carrier gas) flow during the cold-gas dynamic-spray process, require the use of numerical procedures to obtain solutions for the governing equations. Numerical solutions, unfortunately, do not enable an easy establishment of the relationships between the gas, process and feed-powder parameters on one side and the gas and the particle velocities at the nozzle exit and the particle impact velocity, on the other. Analytical solutions for the governing equations in the limits of small and large relative particle/gas velocities and a multiple non-linear regression analysis are used, in the present work, to develop analytical functions which can be used to compute the gas and the particle exit velocities and the particle impact velocity for a given set of the gas, process, and feed-powder parameters. The results obtained using the analytical functions are found to be in a very good agreement with their numerical and experimental counterparts.

15. SUBJECT TERMS

16. SECURITY CLASSIFICATION OF:			17. LIMITATION OF ABSTRACT	18. NUMBER OF PAGES	19a. NAME OF RESPONSIBLE PERSON
a. REPORT **unclassified**	b. ABSTRACT **unclassified**	c. THIS PAGE **unclassified**	**Same as Report (SAR)**	**9**	

Nomenclature

A	nozzle cross-section area
C	specific heat
C_D	drag coefficient
D	drag force
h	convective heat transfer coefficient
L	thickness of the stagnant region
m	mass
$\dot{m}$	mass flow rate
P	pressure
R	gas constant
Re	Reynolds number
S	molecular speed ratio
T	temperature
v	velocity
x	axial distance from the nozzle throat
μ	viscosity
γ	specific heat ratio
ρ	density

Subscripts

o	stagnation quantity
e	nozzle-exit related quantity
p	particle quantity
s	shock related quantity

Superscripts

*	nozzle throat quantity
impact	impact related quantity
opt	optimal quantity
st	stagnant region related quantity

promotes bonding. This theory is supported by a number of experimental findings such as: (a) a wide range of ductile (metallic and polymeric) materials can be successfully cold-sprayed while non-ductile materials such as ceramics can be deposited only if they are co-cold-sprayed with a ductile (matrix) material [2]; (b) the mean deposition particle velocity should exceed a minimum (material-dependent) critical velocity to achieve deposition which suggests that sufficient kinetic energy must be available to plastically deform the solid material and/or disrupt the surface film [3]; and (c) the particle kinetic energy at impact is typically significantly lower than the energy required to melt the particle suggesting that the deposition mechanism is primarily, or perhaps entirely, a solid-state process [4–8].

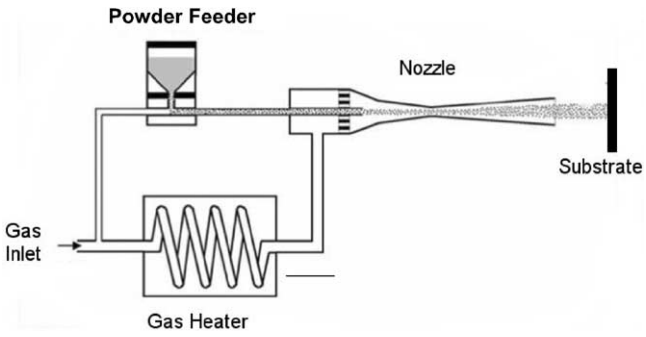

Fig. 1. Schematic of a typical cold-gas dynamic-spray system.

As the cold-spray process does not normally involve the use of a high-temperature heat source, it generally offers a number of advantages over the thermal-spray material deposition technologies such as high velocity oxy-fuel, detonation gun, plasma spray, and arc spray. Among these advantages, the most important appear to be: (a) the amount of heat delivered to the coated part is relatively small so that microstructural changes in the substrate material are minimal or nonexistent; (b) due to the absence of in-flight oxidation and other chemical reactions, thermally- and oxygen-sensitive depositing materials (e.g. copper or titanium) can be cold sprayed without significant material degradation; (c) nanophase, intermetallic and amorphous materials, which are not amenable to conventional thermal spray processes (due to a major degradation of the depositing material), can be cold sprayed; (d) formation of the embrittling phases is generally avoided; (e) macro- and micro-segregations of the alloying elements during solidification which accompany conventional thermal spray techniques and can considerably compromise materials properties do not occur during cold spraying. Consequently, attractive properties are retained in cold-sprayed bulk materials; (f) "peening" effect of the impinging solid particles can give rise to potentially beneficial compressive residual stresses in cold-spray deposited materials [3] in contrast to the highly detrimental tensile residual stresses induced by solidification shrinkage accompanying the conventional thermal-spray processes; and (g) cold spray of the materials like copper, solder and polymeric coatings offers exciting new possibilities for cost-effective and environmentally-friendly alternatives to technologies such as electroplating, soldering and painting [9].

The solid-state particle-bonding mechanism discussed above suggests and experimental observations [9] confirm that it is desirable to maximize the velocity at which feed-powder particles impact the target surface. While, in general, this can be accomplished by increasing the inlet pressure of the carried gas, for practical and economic reasons, it is desirable to maximize the particle impact velocity at a given level of the carrier-gas inlet pressure by properly selecting the type of the carrier gas, its inlet temperature and by optimizing the shape of the converging/diverging cold-spray nozzle. A detailed analysis of the effects that the type of the carrier gas, the inlet gas temperature and the shape of the cold-spray nozzle have on the impact velocity of the feed-powder particles is carried out by Dykhuizen and Smith [10] using an isentropic, one-dimensional gas-flow model. In our recent work [11], the analysis of Dykhuizen and Smith [10] was extended in order to include the effects of finite values of the particle velocity and the effect of

variability of the gas/particle drag coefficient. While the one-dimensional model of Dykhuizen and Smith [10] has been found to be quite successful, its numerical nature does not enable an easy establishment of the relationships between the gas, process and feed-powder parameters on one side and the gas and the particle velocities at the nozzle exit and the velocity at which particles impact the substrate surface, on the other. The objective of the present paper is to use the results of the one-dimensional model by Dykhuizen and Smith [10] and a multiple regression analysis to develop analytical functions which can be used to compute the gas and the particle exit velocities for a given set of the gas, process and feed-powder parameters.

The organization of the paper is as follows: A brief overview of the one-dimensional isoentropic gas flow model developed by Dykhuizen and Smith [10] utilized in the present work is presented in Section 2. The one-dimensional particle dynamics model also proposed by Dykhuizen and Smith [10] is briefly discussed in Section 3. The derivation of the analytical functions for gas and powder-particle velocities at the nozzle exit and for the impact particle velocity are presented in Sections 4.1–4.3, respectively. The key conclusions resulted from the present study are summarized in Section 5.

2. Isentropic gas flow model

In this section, a brief overview is given of the cold-spray gas-flow model developed by Dykhuizen and Smith [10]. The model considers a typical geometry of the cold-spray converging/diverging nozzle (Fig. 1) and involves a number of assumptions and simplifications such as: (a) the gas flow is assumed to be one dimensional and isentropic (adiabatic and frictionless); (b) the gas is treated as a perfect (ideal) gas; and (c) the constant-pressure and the constant-volume specific heats of the gas are assumed to be constant.

The carrier gas flow is assumed to originate from a large chamber or duct where its velocity is zero and the pressure (referred to as the "stagnation" pressure) is P_o and the temperature (referred to as the "total" gas temperature) is T_o. The cold-spray process is furthermore assumed to be controlled by the user who can set the total temperature and the mass flow rate of the gas. The corresponding stagnation pressure can then be calculated using the following procedure:

Using basic dynamic and thermodynamic relations for the compressible fluid flow, the gas temperature T^* at the smallest cross-sectional area of the converging/diverging nozzle (referred to as the nozzle throat in the following) where the Mach number (the velocity of the gas divided by the local speed of sound) is unity, can be derived as [12]:

$$T^* = \frac{T_o}{(1+\gamma-1/2)} \tag{1}$$

where γ is the ratio of the constant-pressure and the constant-volume specific heats which is typically set to 1.66 for monoatomic gases like helium and 1.4 for diatomic gases like nitrogen and oxygen, respectively. Since air is primarily a mixture of nitrogen and oxygen, it is considered as a diatomic gas. γ takes on values smaller than 1.4 in multi-atom molecular gases but such gases are rarely used in the cold-spray process.

The gas velocity at the nozzle throat is equal to the speed of sound and is defined as:

$$v^* = \sqrt{\gamma R T^*} \tag{2}$$

where R is the gas constant (the universal gas constant divided by the gas molecular weight). It should be noted that the superscript * is used throughout this paper to denote the quantities at the nozzle throat, that is the gas quantities under the sonic conditions. Eq. (2) can be used to explain the experimental finding that the low molecular weight (and, hence, large R), monoatomic (and, hence, large γ and, in turn, high T^*) helium is a better carrier gas than the high molecular weight, diatomic air since for the same total gas temperature T_o, it is associated with a higher speed of sound.

From the known (user selected) mass flow rate, $\dot{m}$, the sonic gas density can be computed as:

$$\rho^* = \frac{\dot{m}}{V^* A^*} \tag{3}$$

where A^* is the (known) cross-sectional area of the nozzle throat.

Next, using the ideal gas law, the gas pressure at the nozzle throat can be determined as:

$$P^* = \rho^* R T^* \tag{4}$$

Once the throat pressure P^* is computed, the stagnation pressure P_o can be calculated using the following isentropic relation:

$$P_o = P^* \left(\frac{T_o}{T^*}\right)^{\gamma/(\gamma-1)} = P^* \left(1+\frac{\gamma-1}{2}\right)^{\gamma/(\gamma-1)} \tag{5}$$

After all the gas-dynamics quantities (T^*, v^*, ρ^*, and P^*) are calculated at the nozzle throat, one can proceed to determine these quantities along the diverging section of the nozzle. Toward that end, the variation of one of the these quantities or the variation of the Mach number or the variation of the nozzle cross-sectional area along the diverging section of the nozzle must be specified. Dykhuizen and Smith [10] considered the case when the variation of the nozzle cross-sectional area A is specified, which then allows determination of the corresponding Mach number M from the following equation:

$$\frac{A}{A^*} = \left(\frac{1}{M}\right)\left[\left(\frac{2}{\gamma+1}\right)\left(1+\frac{\gamma-1}{2}M^2\right)\right]^{\gamma/(2\gamma-1)} \tag{6}$$

Once the Mach number is determined at a given cross-sectional area of the diverging section of the nozzle, the remaining corresponding gas quantities (P, T, v, and ρ)

can be calculated using the following isentropic relationships:

$$P = P^* \left(\frac{\gamma + 1}{2 + (\gamma - 1)M^2} \right)^{\gamma/(\gamma-1)} \tag{7}$$

$$T = \frac{T_o}{(1 + (\gamma - 1/2)M^2)} \tag{8}$$

$$v = M\sqrt{\gamma RT} \tag{9}$$

$$\rho = \frac{\rho_o}{(1 + (\gamma - 1)/2)M^2)^{1/(\gamma-1)}} \tag{10}$$

Eqs. (7)–(10) can be used to compute P, T, v, and ρ at the nozzle exit, if the given exit cross-sectional area A_e is substituted for A in Eq. (6). However, it must be noted that P, T, V, and ρ defined in this way will reflect the true conditions of the gas at the nozzle exit only if a normal shock does not take place inside the nozzle. To determine if the normal shock will take place inside the nozzle, the ambient pressure should be compared with the following "shock" pressure:

$$P_s = P_e \left(\frac{2\gamma}{\gamma + 1} M_e^2 - \frac{\gamma - 1}{\gamma + 1} \right) \tag{11}$$

where subscript e is used to denote the gas quantities at the nozzle exit.

If the shock pressure P_s is lower than the ambient pressure, a shock will occur inside the nozzle and the subsequent gas flow is subsonic so that the exit pressure is not given by Eq. (7), but it is rather equal to the ambient pressure. Under normal cold-spray operating conditions, the shock pressure is maintained above the ambient pressure so that no shock occurs inside the nozzle and the exit pressure is defined by Eq. (7). At the same time, the exit gas pressure, P_e, is generally lower than the ambient pressure in effort to maximize the exit velocity of the gas (and thus, the average velocity of the feed-powder particles, referred to as the particle velocity in the following). Under such conditions, the one-dimensional gas dynamics model developed by Dykhuizen and Smith [10] and briefly reviewed above can be used to analyze the gas flow inside the nozzle. As the gas leaves the nozzle, it slows down as the gas pressure tries to adjust to the ambient pressure. However, due to a relatively short nozzle-exit/substrate-surface standoff distance encountered in the cold-spray process, this decrease in the gas velocity is not expected to be significant. However, the impingement of the gas jet upon the substrate surface gives rise to the formation of a bow shock (stagnant) region in front of the substrate. The component of the gas velocity normal to the substrate surface in this region is quite small relative to the nozzle-exit gas and particle velocities. In addition, the gas flow in this region is dominated by its lateral component. A more detailed discussion of the stagnant region and its effect of the particle impact velocity is presented in Section 4.3.

3. Particle dynamics model

Dykhuizen and Smith [5] also analyzed the interactions of the carrier gas with the spray particles under the approximation of a dilute two-phase (gas + non-interacting solid particles) flow. The particle velocity, v_p, can, in this case, be determined by solving the following differential equation:

$$m_p \frac{dv_p}{dt} = m_p v_p \frac{dv_p}{dx} = \frac{C_D A_p \rho (v - v_p)^2}{2} \tag{12}$$

where m_p and A_p are the average mass and the cross-sectional area of the particles, respectively, C_D the drag coefficient, t the time and x the axial distance traveled by the particle (measured from the nozzle throat). Under the condition of constant gas velocity, gas density and drag coefficient, Eq. (12) can be integrated to yield:

$$\log\left(\frac{v - v_p}{v} \right) + \frac{v}{v - v_p} - 1 = \frac{C_D A_p \rho x}{2 m_p} \tag{13}$$

It should be noted that Eq. (13) may generally not be valid since both the gas density and the drag coefficient may vary over the length of the nozzle [10,11].

A simple analysis of Eq. (12) shows that the ultimate particle velocity is equal to the gas velocity. Furthermore, examination of Eqs. (6), (8) and (9) indicates that the gas velocity within the nozzle depends on the total gas temperature and the nozzle geometry (i.e. the cross-sectional area at a given axial distance x), but not on the gas pressure (under the condition of a constant drag coefficient). However, Eqs. (9), (10) and (12) indicate that the initial particle acceleration (dv_p/dt at $v_p = 0$) is linearly dependent on the stagnation pressure but independent of the total temperature. Thus, while the stagnation pressure does not affect the maximum particle velocity, it has to be sufficiently high to ensure that the spray-particles velocity will approach the gas velocity over a relatively short length of the diverging section of the nozzle.

4. Results and discussion

4.1. Gas velocity at the nozzle exit

As discussed in the Section 2, the gas velocity at the nozzle exit can be computed using the one-dimensional numerical model of Dykhuizen and Smith [10]. However, this model entails the solution of a non-linear algebraic equation, Eq. (6), and does not enable an easy access to the relationships between the carrier-gas and the cold-spray process parameters on one side and the gas velocity at the nozzle exit, on the other.

An attempt was made in this section to construct an analytical function which can be used to compute the gas exit velocity for a given set of gas and process parameters. Towards that end, Eq. (6) is solved for the Mach number M for different values of the nozzle expansion ratio, A/A^*, and

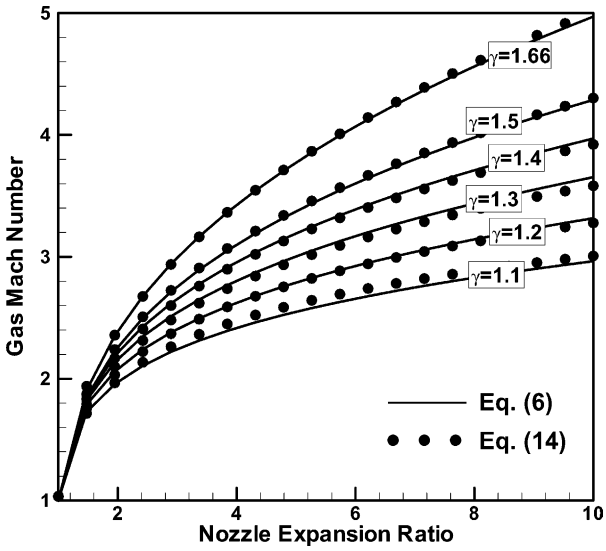

Fig. 2. Variation of the gas Mach number with the nozzle expansion ratio and the gas specific-heat ration, γ.

for several values of the specific heat ratio, γ. The results obtained are displayed as solid lines in the Fig. 2. Next, a non-linear least squares procedure is used to fit the M versus A/A^* data for different γ values to a function:

$$M = \left[k_1 \frac{A}{A^*} + (1 - k_1)\right]^{k_2} \tag{14}$$

where k_1 and k_2 are function of the specific heat ratio, γ. A non-linear polynomial regression analysis is next used to establish the γ-dependence of k_1 and k_2 as:

$$k_1 = 218.0629 - 243.5764\gamma + 71.7925\gamma^2 \tag{15}$$

$$k_2 = -0.122450 + 0.281300\gamma \tag{16}$$

A comparison of the M versus A/A^* relation defined by Eq. (14), and the one predicted by the model of Dykhuizen and Smith [10], Eq. (6), is shown in Fig. 2. The M versus A/A^* data based on Eq. (14) are shown as solid circles in Fig. 2. A reasonably good agreement is seen between the two sets of results particularly for high γ values encountered in mono-atomic (e.g. helium) and di-atomic (e.g. air, nitrogen) gases commonly used in the cold-spray process.

Next Eq. (8) is substituted in Eq. (9) to obtain:

$$v = M\sqrt{\frac{\gamma R T_o}{1 + (\gamma - 1/2)M^2}} \tag{17}$$

Thus Eq. (17), in conjunction with Eqs. (14)–(16), can be used to compute the exit gas velocity v_e as a function of the nozzle exit expansion ratio, (A_e/A^*), and the carrier-gas (stagnation) properties: γ, R, and T_o.

4.2. Particle velocity at the nozzle exit

The non-linear first-order ordinary differential equation, Eq. (12), does not have an analytical (closed form) solution over the entire range of nozzle lengths, $0 < x < \infty$. Therefore, a numerical integration routine must be used to solve Eq. (12). While an integration procedure can be readily implemented, the numerical solution for the v_p versus x relationship obtained is not very attractive, since it does not offer an insight into the effect of various carrier gas, process, and feed-powder parameters. To overcome this limitation, analytical solutions for Eq. (12) are first sought in two distinct limits: (a) $v_p \ll v$ and (b) $v_p \approx v$.

When the particle velocity is small in comparison with the gas velocity, and the changes in gas density are negligible (ρ = constant), Eq. (12) can be solved to yield:

$$v_p = v\sqrt{\frac{3\rho C_D x}{\rho_P D_p}} \tag{18}$$

where the gas density is given in terms of the stagnation gas density, ρ_o, and the Mach number, M, via Eq. (10), while ρ_o is related to the stagnation pressure, P_o, and the total gas temperature, T_o, via Eq. (4). As will be demonstrated later in this section, by comparing model predictions with their experimental counterparts the ρ = constant assumption used in the derivation of Eq. (18) is found to be justified.

When the particle velocity is comparable with the gas velocity, (i.e. when the relative particle/gas Reynolds number is small), the particle velocity gradient is defined as:

$$\frac{dv_p}{dx} = \frac{18\mu(v - v_p)}{v D_p^2 \rho_p} \tag{19}$$

where μ is the gas viscosity which enters Eq. (19) through a relationship between the drag coefficient and the relative Reynolds number. Integration of Eq. (19) yields:

$$v_p = v\left\{W_0\left[-\exp\left(-\frac{18\mu x}{D_p^2 \rho_p v} - 1\right)\right] + 1\right\} \tag{20}$$

where W_0 is the principal branch of the Lambert W function.

The Lambert W function is defined as the function that solves the equation $W(z)e^{W(z)} = z$ where z is a real or a complex number. Since this equation always has an infinite number of solutions, most of them complex, $W(z)$ is a multi-valued function. The different possible solutions are labeled by an integer variable k called the branch of $W(z)$. Thus, the proper way to talk about the solutions of the equation $W(z)e^{W(z)} = z$ is to say that they are: $W_k(z)$ where $k = 0, \pm1, \pm2$, etc. When z is a real number and $z < -1/e$, the solution to the equation $W(z)e^{W(z)} = z$is multi-valued and complex. When $-1/e \le z < 0$ there are two possible real values of $W(z)$. The branch satisfying $W(z) \ge -1$ is denoted as $W_0(z)$ and is called the *principal branch*. The branch satisfying $W(z) < -1$ is denoted as $W_{-1}(z)$. When z is real and $z \ge 0$, the solution to the equation $W(z)e^{W(z)} = z$ is single-valued and real and belongs to the principal branch, $W_0(z)$. The real solution of the equation $W(z)e^{W(z)} = z$ are displayed in Fig. 3. It is the portion of the principal branch for $-1/e \le z < 0$ which is of interest in the present work since for $0 \le x < \infty$ the magnitude of the Lambert function

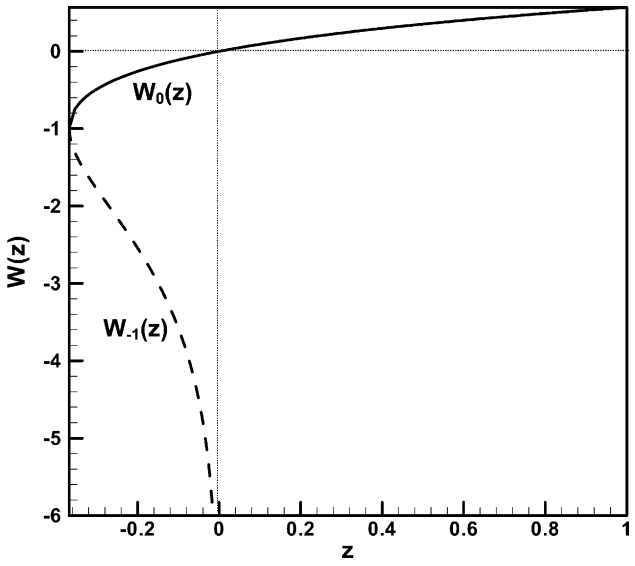

Fig. 3. Real branches of the Lambert *W* function.

should change between −1 and **0** (to ensure that v_p changes between 0 and v) and for x=0, the argument of the function $W_0(z)$ in Eq. (20) is equal to $-1/e$ while for x becoming infinite the argument of the function $W_0(z)$ in Eq. (20) is zero. The Lambert *W* function is implemented in many commercial general-purpose computing systems such as Matlab (used in the present work), Maple, Macsyma, and Mathematica. For $-1/e \le z \le 0$, of interest in the present work, $W_0(z)$ can be approximated using the following nonlinear function:

$$m_1 = -e^{-1} \qquad m_2 = -e^{-9} \qquad m_3 = -2e$$

$$s_1 = \sqrt{2} \qquad s_2 = 2s_1 - 3 \qquad s_3 = 4 - 3s_2 \qquad s_4 = s_1 - 2$$

$$W_0(z) = \alpha / \left[1 + \left\{ \alpha / \left(3 + \frac{\alpha(s_2\beta + s_3)}{s_4(\alpha + \beta)} \right) \right\} \right] - 1 \qquad (21)$$

Particle velocities normalized by the gas velocity, v_p/v, as a function of the length of the diverging section of the nozzle, x, as predicted by Eqs. (18) and (20), are plotted in Fig. 4 (curves labeled "Eqs. (18) and (20)"). Eq. (18) is used at low values of x where the v_p/v values are small while Eq. (20) is used at large values of x where the v_p/v values are near unity. The following (typical) cold-spray processing conditions are used to generate the results presented in Fig. 4: carrier gas—helium, the total gas temperature T_o = 600 K, the stagnation pressure P_o = 22 bar, gas viscosity $\mu = 1.9 \times 10^{-5}$ Ns/m^2; the mean particle diameter D_P = 10 μm and the particle material density ρ_p = 2.7 g/cm^3. The variation of v_p/v with x obtained using the one-dimensional numerical model of Dykhuizen and Smith [10] is also shown in Fig. 4 (curve labeled "Numerical"). It is seen that the analytical solution given by Eq. (18) agrees quite well with the numerical solution in the regions of its validity. The same holds for the analytical solution given by Eq. (20), but at very large x values. Since such x values are not of practical interest in the cold-gas dynamic-spray process, they are not shown in Fig. 4.

To construct an analytical v_p/v versus x function for the entire $0 \le v_p/v \le 1$range, it is next assumed that the v_p/v versus x relationship for the intermediate v_p/v values can be obtained as a linear combination of the two relations predicted by Eqs. (18) and (20). However, before such linear combination is constructed, the two v_p/v versus x functional relations predicted by Eqs. (18) and (20) are respectively transformed into the following exponential forms:

$$\left(\frac{v_p}{v}\right)_{18} = -e^{-\sqrt{3\rho C_D x/\rho_p D_p}} + 1 \qquad v_p \ll v \qquad (22)$$

$$\left(\frac{v_p}{v}\right)_{20} = -e^{-9\mu x/D_p^2 \rho_p v} + 1 \qquad v_p \approx v \qquad (23)$$

Eqs. (22) and (23) are next combined as:

$$\frac{v_p}{v} = w\left(\frac{v_p}{v}\right)_{18} + (1-w)\left(\frac{v_p}{v}\right)_{20} \qquad (24)$$

where w and $1 - w$ are the weighting factors. In principle, optimal values of the weighting factors can be obtained by minimizing deviations of the v_p/v versus x relation predicted by Eq. (24) from the numerical solution. This is not done in the present work to avoid unnecessary complexities associated with the dependence of such optimal values on various gas, process and feed-powder parameters. A value of $w = 0.5$ is found to give a reasonably good agreement between the v_p/v versus x relation predicted by Eq. (24) and its numerical counterpart for a wide range of gas, process and feed-powder parameters. A typical level of agreement between the v_p/v versus x relation predicted by Eq. (24) (denoted as "Eq. (24)") and its numerical counterpart (denoted as "Numerical") is shown in Fig. 4.

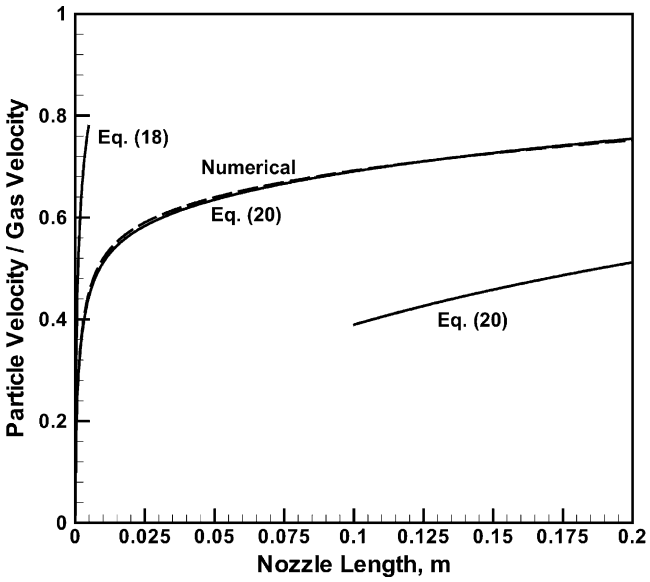

Fig. 4. Variation of the ratio of the particle velocity and the gas velocity at the nozzle exit with length of the nozzle. Please see text for details.

Thus, Eq. (24), in conjunction with Eqs. (22) and (23), can be used to compute the particle velocity at the nozzle exit for a given set of the gas parameters: γ, μ, R, T_o, and P_o; the process parameters: A/A^* and x; and the feed-powder parameters: ρ_p and D_p.

4.3. Particle impact velocity

As discussed in Section 2, calculations of the velocity of the velocity at which feed-powder particles impact the substrate surface must include the effects associated with the impingement of the supersonic gas jet upon the substrate. Supersonic impinging jets have been the focus of research for over three decades because of their application in a number of diverse areas ranging from hovering of the short takeoff and vertical landing (STOVL) aircrafts to material processing (e.g. the cold-gas dynamic-spray process). While fluid dynamics and acoustic properties of the supersonic impinging jets vary considerably with the geometrical parameters of the nozzle, the distance between the nozzle exit and the substrate, the exit Mach number, etc., some common global features of the supersonic impinging jets can be identified. A schematic of the supersonic impinging jet flowfield is given in Fig. 5. It is seen that the impinging jet flowfield can be divided into three main regions [13]. The first region represents the main jet column in which the flow is primarily inviscid and contains expansion and compression shock waves for non-ideally expanding jets. The second region, generally referred as the impinging zone, involves the region of jet impingement onto the substrate. The impingement zone is characterized by large gradients which cause major changes in the local flow properties. A stagnation bubble containing re-circulating fluid with relatively low velocity is also depicted within the impingement region in Fig. 5. The origin of this bubble is not well understood. Nevertheless, its presence is found to affect pressure distribution over the substrate surface. The third region, known as the radial wall jet, includes the area outside the impingement zone which contains the jet flow, redirected laterally outward after impingement. As the supersonic flow in the primary jet approaches the substrate, it decelerates through the formation of a bow shock. If the jet is not ideally expanded, oblique shocks in the jet plume (denoted as "jet shocks" in Fig. 5) interact with the bow shock resulting in the so-called "triple-shock structure", with the third shock denoted as a "tail shock" in Fig. 5. The interaction between the three shocks is believed to govern the flowfield in the impingement zone [14].

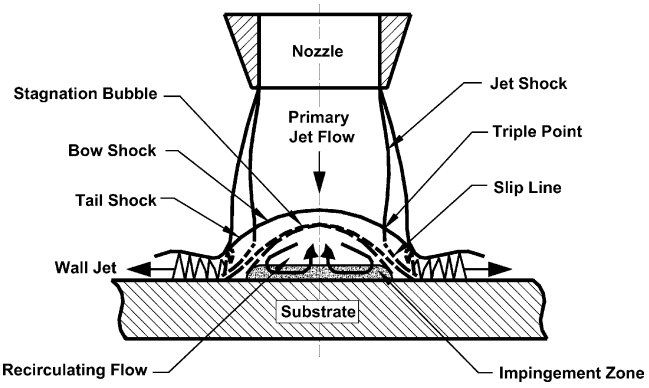

Fig. 5. Schematic of a supersonic impinging jet flow field.

A computational analysis of the impinging supersonic jet entails finding the solution to the following governing differential equations:

- Reynolds averaged Navier–Stokes equations which include the momentum conservation equations and a continuity equation for compressible turbulent fluid low;
- An energy conservation equation;
- Closure relations which enable evaluation of the velocity-fluctuations based terms (called the Reynolds stress tensor) in the Reynolds averaged Navier–Stokes and the energy conservation equations. Among various models for the closure relationship, one-equation Spalart model [15], and two-equation model (e.g. the k-ϵ model [16], the k-ω model [17], and the shear-stress transport (SST) model [18]) are most frequently used; and
- Constitutive relations such as the ideal-gas law, the Sutherland's law for the temperature-dependence of the (laminar) gas viscosity, and the models for the molecular and the turbulent Prandtl number.

In our ongoing work, FEMLAB general-purpose finite-element computer program [19] is used to analyze the flowfield in supersonic axisymmetric impinging jets. The objective of this work is to establish relationships between the primary-jet characteristics (more precisely the carrier-gas characteristics at the nozzle exit) and the flowfield in the stagnant zone behind the bow shock adjacent to the substrate. While a detail account of this work will be reported in a future correspondence, some of the results obtained will be utilized here to help construct an analytical function which relates the primary-jet and the geometrical parameters and the flowfield of a stagnant zone adjacent to the substrate surface.

In accordance with many previous experimental and computational analyses, our work shows that the gas flow is subsonic in the stagnant region and that the component of the gas velocity normal to the substrate surface is quite small in comparison with the gas and particle exit-velocities. Under such condition Eq. (12), can be integrated to yield the particle impact velocity as [20]:

$$v_p^{\text{impact}} = v_p e^{-3\rho^{st}L^{st}/4\rho_p D_p} \tag{25}$$

where ρ^{st} is the average gas density in the stagnant region while L^{st} is thickness of this region. In our ongoing work, the following relationships were found for ρ^{st} and L^{st}.

$$\rho^{st} = o_e(-1.04 + 2.27M_e - 0.21M_e^2) \tag{26}$$

$$L^{st} = R_e(0.97 - 0.02M_e) \qquad 1 \le M_e \le 5 \tag{27}$$

where M_e is the gas Mach number at the nozzle exit. Thus, Eq. (23), in conjunction with Eqs. (22)–(24), can be used to compute the impact particle velocity for a given set of (stagnation) gas, process and feed powder parameter. In addition, as suggested by Dykhuizen [20]. Eq. (25) in conjunction with. Eqs. (22)–(24), can be used to determine the optimum particle size distribution. That is, if particles are too large (and heavy), they will not be accelerated enough with the nozzle, but their deceleration within the stagnant region will be modest. When the particles are too small (and light), on the other hand, they will acquire a high exit velocity but may be greatly decelerated within the stagnant zone. Consequently, the impact velocities of particles which are either too large and too heave or too small and too light will be relatively low and the maximum impact velocities will be attained by particles of an optimum size (and weight). This can be seen in Fig. 6 in which the effect of the particle size, the gas type and the feed-powder particle size on the particle impact velocity is shown. The results displayed in this figure show that: (a) the particle size which is associated with the largest impact velocity scales with an inverse of the feed-powder density; (b) the maximum particle impact velocities for the two feed powders (copper and aluminum) are very close to each other for either choice of the carrier gas (helium or air); and (c) helium gives rise to a substantially higher particle impact velocities. All these findings are consistent with the results of Dykhuizen [20]. Also displayed in Fig. 6 are the experimental results for the impact velocity of copper particles with 1 μm diameter accelerated in air and with 20 μm diameter accelerated in helium [21]. Due to the observed relatively good agreement between the experimental results and the corresponding model prediction displayed in Fig. 6, one might conclude that one of the key simplifications used in the development of the model involving the neglect of variations of the gas density and the drag coefficient along the diverging section of the nozzle was justified.

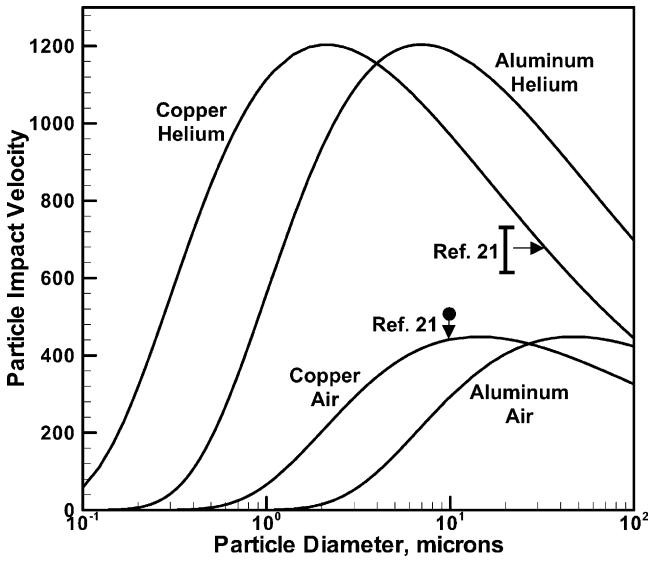

Fig. 6. Effect of the particle size, the feed-powder material and the carrier gas on the particle impact velocity.

5. Conclusions

Based on the results obtained in the present work, the following main conclusions can be drawn. (1) Using a nonlinear regression analysis and a numerical solution for the one-dimensional isentropic gas flow in a cold-gas dynamic-spray nozzle, a relatively simple function is defined which relates the gas velocity at the nozzle exit with the nozzle expansion ratio and the carrier gas stagnation properties. (2) Analytical solutions for the particle velocity at the nozzle exit in the limits of very short and very long nozzle lengths can be combined to derive an analytical function which relates the particle velocity at the nozzle exit for intermediate nozzle lengths with various gas, process and feed-powder parameters. (3) To compute the velocity at which particles impact the substrate surface, deceleration of the particles in a stagnant subsonic region adjacent to the substrate surface must be considered.

Acknowledgements

The material presented in this paper is based on work supported by the US Army Grant Number DAAD19-01-1-0661. The authors are indebted to Drs. Walter Roy and Fred Stanton of the ARL for the support and a continuing interest in the present work. The authors also acknowledge the support of the Office of High Performance Computing Facilities at Clemson University.

References

[1] A.P. Alkhimov, A.N. Papyrin, V.F. Dosarev, N.I. Nestorovich, M.M. Shuspanov, Gas dynamic spraying method for applying a coating, US Patent 5,302,414, 12, April 1994.
[2] A.O. Tokarev, Met. Sci. Heat. Treat. 35 (1996) 136.
[3] R.C. McCune, A.N. Papyrin, J.N. Hall, W.L. Riggs, P.H. Zajchowski, in: C.C. Berndt, S. Sampath, (Ed.), An exploration of the cold gas-dynamic spray method for several material systems, Thermal Spray Science and Technology, ASM International, 1995, pp. 1–5.
[4] J. Vlcek, A systematic approach to material eligibility for the cold spray process, in: International Thermal Spray Conference and Exhibition, May 5–8, Orlando, 2003, Florida, USA.
[5] D.G. McCartney, Particle-substrate interactions in cold gas dynamic spraying, in: International Thermal Spray Conference and Exhibition, May 5–8, Orlando, 2003, Florida, USA.
[6] M. Grujicic, J.R. Saylor, D.E. Beasley, W.S. DeRosset, D. Helfritch, Computational analysis of the interfacial bonding between feed powder particles and the substrate in the cold-gas dynamic-spray process, Appl. Surf. Sci. 219 (2003) 211–327.
[7] H. Assadi, F. Gärtner, T. Stoltenhoff, H. Kreye, Acta Mater. 51 (2003) 4379.
[8] F. Gärtner, Numerical and microstructural investigations of the bonding mechanisms in cold spraying, in: International Thermal Spray Conference and Exhibition, May 5–8, 2003, Orlando, Florida, USA.

[9] C.V. Bishop, G.W. Loar, Plat. Surf. Finish 80 (1993) 37.
[10] R.C. Dykhuizen, M.F. Smith, J. Therm. Spray Technol. 7 (1998) 205.
[11] M. Grujicic, W.S. DeRosset, D. Helfritch, Flow analysis and nozzle-shape optimization for the cold-gas dynamic-spray process, materials and design, J. Eng. Manufact., August, 2003, in press.
[12] J.D. Anderson, Fundam. Aerodyn., McGraw Hill, New York, NY, 2001.
[13] C.P. Donaldson, R.S. Snedeker, J. Fluid Mech. 45 (1971) 281.
[14] G.T. Kalghatgi, B.L. Hunt, Aeronautic. Q. 27 (1976) 169.
[15] P.R. Spalart, S.R. Allmaras, AIAA, Paper 92-0439, January 1992.
[16] W.P. Jones, B.E. Launder, Int. J. Heat Mass Transfer 16 (1973) 1119.
[17] D.C. Wilcox, AIAA J. 26 (1988) 1299.
[18] F.R. Menter, AIAA Paper 93-2906, July 1993.
[19] http://www.comsol.com, FEMLAB 2.3a, COMSOL Inc., Burlington, MA 01803, 2003.
[20] R.C. Dykhuizen, Optimizing the cold spray process, in: International Thermal Spray Conference and Exhibition, May 5–8, Orlando, 2003, Florida, USA.
[21] D.L. Gilmore, R.C. Dykhuizen, R.A. Neiser, T.J. Roemer, M.F. Smith, J. Therm. Spray Technol. 8 (1999) 576.